AFRL-RX-WP-TR-2024-0046

MORPHOLOGY CONTROLLED FABRICATION OF RARE EARTH MAGNETIC MATERIALS USING ENGINEERED BIOSYSTEMS

Bedford M. Nicholas
The University of New South Wales

30 APRIL 2024
Final Report

THIS IS A SMALL BUSINESS INNOVATION RESEARCH (SBIR) PHASE I REPORT

AIR FORCE RESEARCH LABORATORY
MATERIALS AND MANUFACTURING DIRECTORATE
WRIGHT-PATTERSON AIR FORCE BASE, OH 45433-7750
AIR FORCE MATERIEL COMMAND
UNITED STATES AIR FORCE

NOTICE AND SIGNATURE PAGE

Using Government drawings, specifications, or other data included in this document for any purpose other than Government procurement does not in any way obligate the U.S. Government. The fact that the Government formulated or supplied the drawings, specifications, or other data does not license the holder or any other person or corporation; or convey any rights or permission to manufacture, use, or sell any patented invention that may relate to them.

Qualified requestors may obtain copies of this report from the Defense Technical Information Center (DTIC) (http://www.dtic.mil).

AFRL-RX-WP-TR-2024-0046 HAS BEEN REVIEWED AND IS APPROVED FOR PUBLICATION IN ACCORDANCE WITH ASSIGNED DISTRIBUTION STATEMENT.

DENNIS.PATRICK.BRIAN.1376889099 Digitally signed by DENNIS.PATRICK.BRIAN.1376889099 Date: 2024.07.02 15:08:50 -04'00'

PATRICK DENNIS
Project Engineer
Biomaterials Branch
Photonics, Electronics & Soft Materials Division
Materials and Manufacturing Directorate

MEADE.MITCHELL.LEE.1362279409 Digitally signed by MEADE.MITCHELL.LEE.1362279409 Date: 2024.07.02 15:11:15 -04'00'

MITCHELL MEADE
Deputy Branch Chief
Biomaterials Branch
Photonics, Electronics & Soft Materials Division
Materials and Manufacturing Directorate

This report is published in the interest of scientific and technical information exchange, and its publication does not constitute the Government's approval or disapproval of its ideas or findings.

REPORT DOCUMENTATION PAGE

Form Approved
OMB No. 0704-0188

1. REPORT DATE *(DD-MM-YYYY)*	**2. REPORT TYPE**	**3. DATES COVERED** *(From - To)*
30 April 2024	FINAL	01 September 2022 – 30 March 2024

4. TITLE AND SUBTITLE

Morphology Controlled Fabrication of Rare Earth Magnetic Materials Using Engineered Biosystems

5a. CONTRACT NUMBER
FA8650-22-2-7219

5b. GRANT NUMBER

5c. PROGRAM ELEMENT NUMBER
61101E

6. AUTHOR(S)

Nicholas M. Bedford, Yuwei Yang

5d. PROJECT NUMBER
DARPA

5e. TASK NUMBER

5f. WORK UNIT NUMBER
X22V

7. PERFORMING ORGANIZATION NAME(S) AND ADDRESS(ES)
The University of New South Wales
2 High Street
Sydney, NSW, 2052

8. PERFORMING ORGANIZATION REPORT NUMBER
AFRL-RX-WP-TR-2024-0046

9. SPONSORING / MONITORING AGENCY NAME(S) AND ADDRESS(ES)
Air Force Research Laboratory
Materials and Manufacturing Directorate
Wright-Patterson Air Force Base OH 45433
Air Force Materiel Command
United States Air Force

10. SPONSOR/MONITOR'S ACRONYM(S)
AFRL/RXEB

11. SPONSOR/MONITOR'S REPORT NUMBER(S)
AFRL-RX-WP-TR-2024-0046

12. DISTRIBUTION / AVAILABILITY STATEMENT
Distribution Statement A: Approved for public release: distribution is unlimited.

13. SUPPLEMENTARY NOTES
Report contains color.

14. ABSTRACT

The core goal of our BIO-INC project is to demonstrate the viability of engineered proteins as templates to create magnetically active rare earth element (REE) nanoparticles by examining relationships between protein structure/functionality, REE chemistry, nanomaterials structure/morphology, and subsequent magnetic properties. Using two different protein templates, filamentous γ-prefoldin (γPFD) and encapsulation protein cages, REE nanoparticles were synthesized onto either wild-type (WT) proteins or those functionalized with previously established REE binding motifs, focusing mostly on Dy-based materials. To date, our best-performing material exceeds the 15-month milestone of saturation magnetization of > 100 emu/g, while our lowest coercivity values are approaching the < 10 Oe 15-month benchmark. Advanced characterization methods, including high resolution (HR) cryo-electron microscopy (Cyro-EM) and advanced synchrotron scattering and spectroscopy experiments, have been integrated into our workflow to help establish synthesis-structure-property relationships to help guide future materials design.

15. SUBJECT TERMS
Magnetically Active Rare Earth Element (REE), Biomineralization, Functionalized Protein, Advanced Characterization

16. SECURITY CLASSIFICATION OF:			**17. LIMITATION OF ABSTRACT**	**18. NUMBER OF PAGES**	**19a. NAME OF RESPONSIBLE PERSON**
a. REPORT	**b. ABSTRACT**	**c. THIS PAGE**			Patrick Dennis
Unclassified	Unclassified	Unclassified	SAR	36	**19b. TELEPHONE NUMBER** *(include area code)* (937) 255-9068

Standard Form 298 (Rev. 8-98)
Prescribed by ANSI Std. Z39.18

TABLE OF CONTENTS

LIST OF FIGURES

Figure **Page**

LIST OF TABLES

Table **Page**

1. EXECUTIVE SUMMARY

The core goal of our BIO-INC project is to demonstrate the viability of engineered proteins as templates to create magnetically active rare earth element (REE) nanoparticles by examining relationships between protein structure/functionality, REE chemistry, nanomaterials structure/morphology, and subsequent magnetic properties. Using two different protein templates, filamentous γ-prefoldin (γPFD) and encapsulation protein cages, REE nanoparticles were synthesized onto either wild-type (WT) proteins or those functionalized with previously established REE binding motifs, focusing mostly on Dy-based materials. To date, our best-performing material exceeds the 15-month milestone of saturation magnetization of > 100 emu/g, while our lowest coercivity values are approaching the < 10 Oe 15-month benchmark. Advanced characterization methods, including high resolution (HR) cryo-electron microscopy (Cyro-EM) and advanced synchrotron scattering and spectroscopy experiments, have been integrated into our workflow to help establish synthesis-structure-property relationships to help guide future materials design.

1.1 Key Findings

- Protein-enabled Dy REE were successfully synthesized and exhibited 296 emu/g magnetization and 28.1 Oe using WT γPFD truncated with the TERM protein to reduce the protein template length. For comparison, Dy mineralized without TERM exhibits lower magnetization (137 emu/g) and higher coercivity (82.0 Oe). The length of γPFD filaments for templating Dy-based REE strongly influences magnetic properties for functionalized γPFD as well. Note all magnetization values have been normalized to the mass of Dy (or other REE) throughout this report.

- Using Dy-based REEs, protein-enabled magnetic properties can be modulated by using different protein templates (γPFD and encapsulin) or by the inclusion of REE binding peptides (LBT). The resulting materials are mixtures of amorphous Dy_2O_3 and nanocrystalline $Dy(NO_3)_3$ for all materials examined thus far as determined using cryo-EM and synchrotron characterization studies.

- Metal K-edge XANES measurements show a correlation between the covalency of the metal-oxygen bond and the saturation magnetization of the Dy-containing biominerals. The results suggest a stronger covalent bond is related to a higher saturation magnetization and can be potentially used as means to explain and eventually establish synthesis-structure-property relationships with further examination.

2. INTRODUCTION

The synthesis and control of rare earth element (REE) magnetic nanomaterials remain a significant challenge in materials science, particularly in achieving precise control over their composition, size, shape, and magnetic properties. Traditional solution-based synthetic techniques, while established, face difficulties in scalability and device integration. To address these limitations, this proposal explores a novel approach leveraging engineered biosystems to manipulate the magnetic properties of REE-containing nanomaterials through bio-enabled synthetic conditions.

In this project, we proposed that the magnetic properties of REE nanomaterials can be finely tuned using rationally engineered proteins. Specifically, we will investigate two types of protein architectures: spherical protein cages (encapsulins) and filamentous protein wires (gamma-prefoldin), both functionalized with materials binding peptides (MBPs). These engineered proteins will direct the formation and morphology of REE-based magnetic nanomaterials, offering precise control over their structural and magnetic characteristics. Biological systems possess a unique ability to assemble materials and tune their structures through complex biotic/abiotic interactions. This biogenic specificity, which traditional synthetic techniques lack, can be exploited to create REE-based magnetic materials with superior properties. By integrating MBPs with protein constructs, we aim to modularly manipulate particle size, shape, and local structure, ultimately optimizing magnetic properties such as magnetization and coercivity. Our goal is to produce REE-based magnetic materials with magnetization exceeding 100 emu/g and coercivity below 10 Oe, suitable for applications in high-density memory devices, magneto-optic sensors, and various defense technologies.

The proposed research is structured into four thrusts:

- Protein Engineering for Morphology-Controlled REE Nanomaterials: Utilizing the natural ability of proteins to self-assemble into architectural templates, we will engineer protein constructs to display MBPs, facilitating the binding and mineralization of REE-based materials into controlled morphologies.

- Bio-enabled Synthesis of REE Nanomaterials and Corresponding Non-Biogenic Analogs: We will synthesize REE-containing magnetic nanomaterials within these protein constructs, exploring various biomineralization conditions. Control reactions with known biomineralization proteins and traditional synthesis techniques will provide comparative data.

- Atomic Scale Structural Characterization: Advanced techniques such as high-resolution transmission electron microscopy (HR-TEM), energy-dispersive X-ray spectroscopy (EDS), electron energy loss spectroscopy (EELS), and synchrotron radiation methods will be employed to elucidate the atomic-scale structure of the synthesized materials.

- Analysis of Protein-Directed Magnetic Properties: The magnetic properties of the synthesized nanomaterials will be comprehensively studied as a function of temperature and magnetic field, providing insights into their magnetic ground states and transitions.

Through this interdisciplinary approach, combining synthetic biology, materials science, and

advanced characterization techniques, we aim to establish a blueprint for the biogenic synthesis of REE-based magnetic materials. The successful outcome of this project is hopefully to pave the way for new research directions and potential commercialization opportunities, significantly advancing the field of magnetic nanomaterials.

3. BIOENGINEERING OF PROTEINS TO TEMPLATE REE-CONTAINING NPS

3.1 Bioengineering of Encapsulin Compartments to Build REE-Containing NPs

DNA sequences encoding encapsulins were chemically synthesized as gBlock gene fragments (IDT) and cloned via Gibson assembly into protein expression plasmids containing an inducible T7lac promoter. Expression was conducted in BL21(DE3) E. coli under isopropyl β-D-1-thiogalactopyranoside (IPTG) induction. Cells were lysed by sonication and clarified by centrifugation, then encapsulin in the supernatant was enriched by fractional precipitation with $(NH_4)_2SO_4$. The resolubilised precipitate was purified by anion-exchange chromatography over a HiPrep Q column to remove nucleic acids, followed by low-resolution size-exclusion chromatography over a Sephacryl S-500 column to remove lipid impurities and protein aggregates, then finally high-resolution size-exclusion chromatography over a Superose 6 column to isolate uniform encapsulin particles. The purity and homogeneity of encapsulins were analyzed by SDS-PAGE (**Figure 1**).

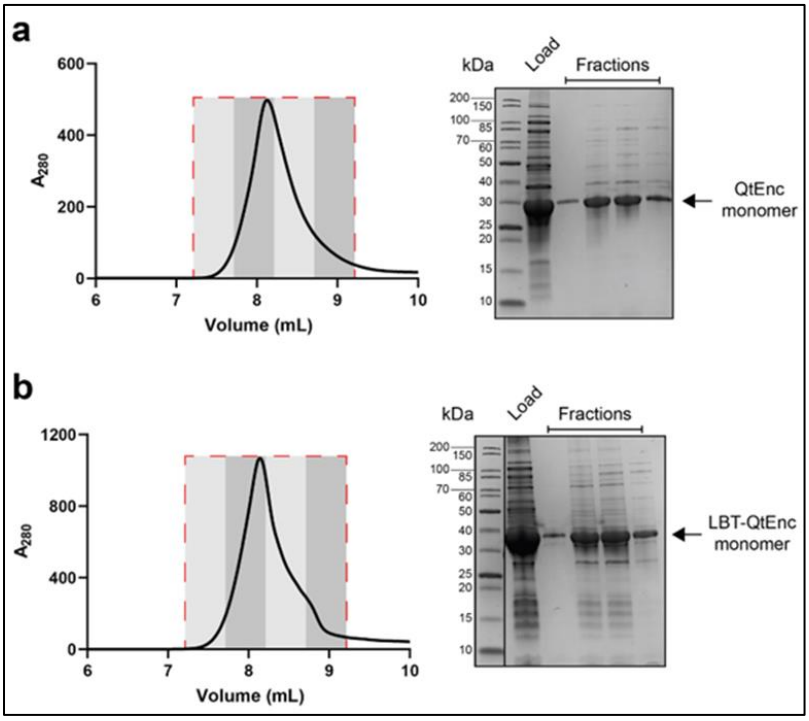

Figure 1. Size-exclusion chromatograms (Superose 6) and accompanying SDS-PAGE analyses for the purification of (a) QtEnc and (b) LBT-QtEnc. The red dotted box indicates fractions from chromatography which were analyzed by SDS-PAGE

Confirmation of particle assembly and size was provided by negative stain TEM. Both QtEnc WT and LBT-QtEnc appeared as monodisperse single particles with an average diameter of 42 nm (**Figure 2**). Some clumping of particles under TEM can be observed, though this is

commonly observed as an artifact of sample preparation on gold grids, staining with uranyl acetate and subsequent drying. Aggregation is not observed in other characterization methods.

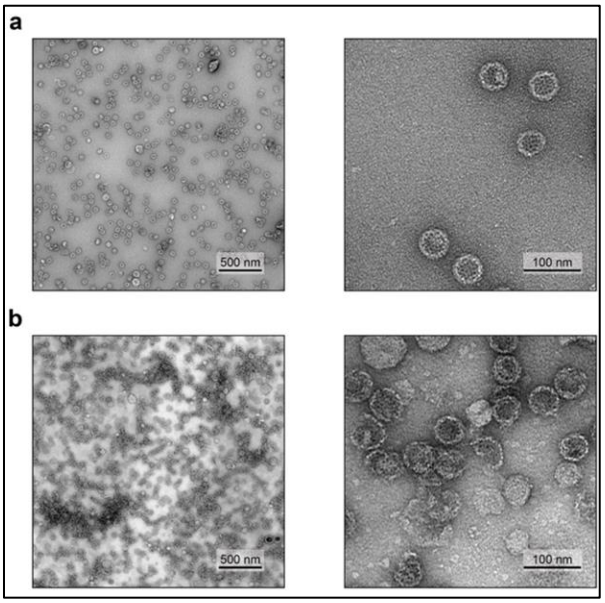

Figure 2. Representative negative stained TEM images showing a wide field and enlarged view of a) QtEnc WT and b) LBT-QtEnc

3.2 Bioengineering of γPFD Filaments to Build REE-Containing NPs

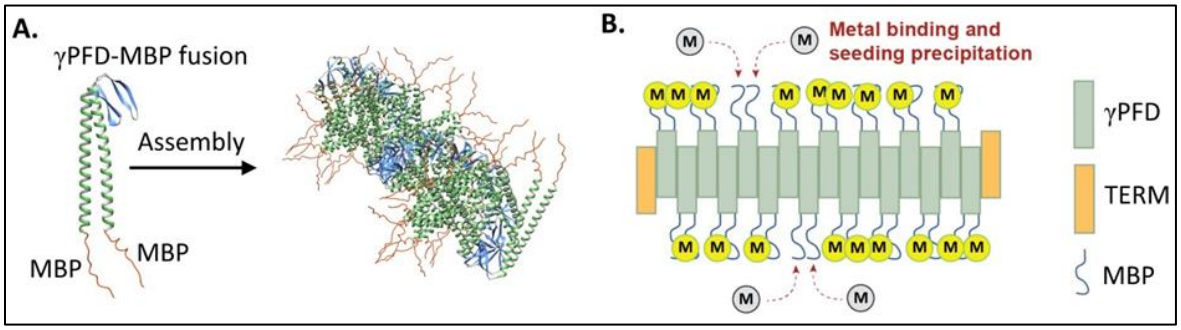

Figure 3. Engineering of γPFD filaments to display material binding peptides (MBPs) for the binding and mineralization of rare earth elements: (A) MBPs were fused to the N-and C-termini of γPFD to enable material binding, (B) Varying the ratio of γPFD to TERM enabled control over filament length.

An ultrastable protein scaffold with tailorable lengths was engineered to enable the binding and mineralization of REEs into nanoparticles of specific dimensions (**Figure 3**, A). The filamentous scaffold is gamma-prefoldin (γPFD) from the archaeon M. jannaschii, which has been used to template a variety of nanomaterials. The length of γPFD filaments can be controlled through the creation of a capping protein called TERM (thermophilic extension resistant mutant). The TERM contains mutations in one of the β-sheet interfaces, which prevents further filament elongation upon TERM incorporation into nascent filaments (**Figure 3**, B). Altering the ratio of γPFD to TERM subunits prior to filament assembly enables tuning of the resulting filament lengths, for example, filaments with uniform 50 ± 5 nm length.

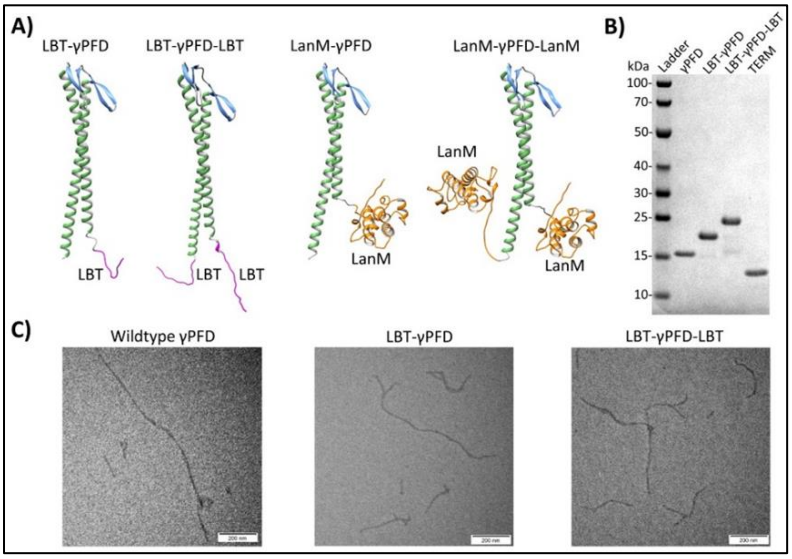

Figure 4. a) Predicted protein structural models for γPFD in fusion with either one or two LBT or LanM REE binding domains. b) SDS-polyacrylamide gel electrophoresis of bacterially expressed and purified wildtype γPFD, variants in fusion with LBT, and the filament capping protein TERM. c) TEM images showing filament morphology of wildtype γPFD, LBT-γPFD, and LBT-γPFD-LBT.

DNA sequences were designed that encode γPFD in fusion with either the LBT or LanM REE-binding sequences at either the N-terminus or both termini of the coiled coil domains of γPFD (**Figure 4**, A). The DNA was commercially synthesized as gene fragments, cloned into plasmid DNA, and transformed into an E. coli protein expression strain. The DNA synthesis company was unable to synthesize the γPFD variant fused to both an N- and C-terminal LanM due to the highly repetitive sequence, and we therefore focused on the other three designs. Both the single and double LBT and the single LanM γPFD fusion proteins were shown to express in E. coli and could be purified via chromatography. In addition, we expressed and purified TERM protein that will be used to control filament length (**Figure 4**, B).

The purified γPFD-LBT and LBT-γPFD-LBT proteins were shown via TEM to assemble as filaments (Figure. 4, C), however, the LanM-γPFD protein did not appear to form filaments. Presumably, the LanM domains caused a steric hinderance for filament self-assembly. Addition of a longer linker sequence between the LanM and γPFD may solve this problem, however, due to time constraints we focused on the two variants of γPFD fused to LBT for REE-mineralization. The filament lengths of the wild-type γPFD and LBT variants in the TEM images were measured, which revealed a Gaussian distribution of lengths with an average length of 296 ± 159 nm for wild-type γPFD, 397 ± 269 nm for γPFD-LBT, and 380 ± 280 nm for the LBT-γPFD-LBT filaments (100 filaments measured for each variant). The γPFD-LBT and LBT-γPFD-LBT filaments were subsequently used for REE binding and mineralization experiments.

3.3 Bioengineering Strategies to Control the Size/Dimensions of REE-Containing NPs

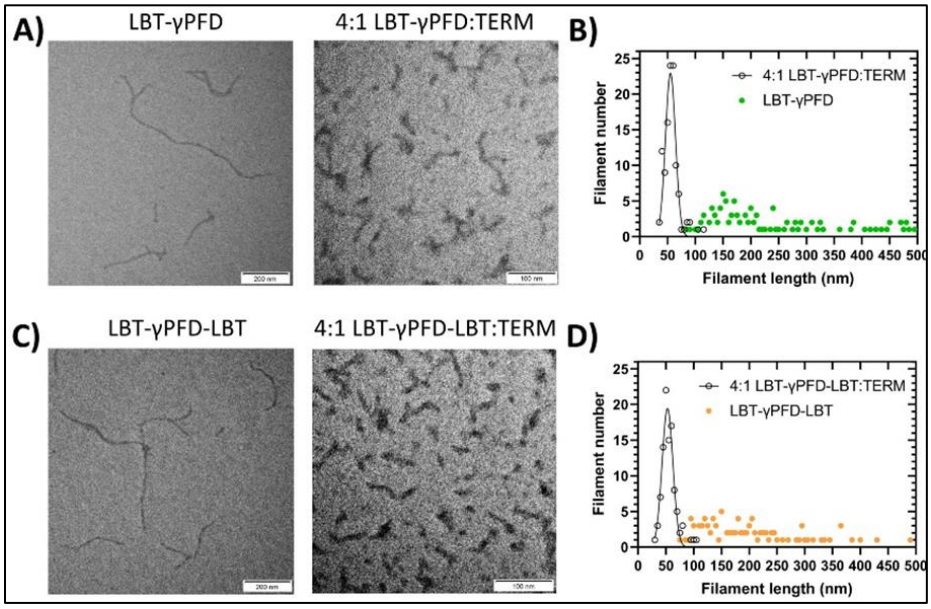

Figure 5. a) TEM images of refolded LBT-γPFD and a mixture of LBT-γPFD:TERM at a 4:1 molar ratio, which were measured and B) plotted as distributions of length (n = 100 filaments). C) TEM images of refolded LBT-γPFD-LBT and a mixture of LBT-γPFD-LBT:TERM at a 4:1 molar ratio, which was measured and D) plotted as distributions of length (n = 100 filaments).

REE-binding filaments of specific lengths were created by assembling either γPFD-LBT and LBT-γPFD-LBT subunits in the presence of the filament-capping protein TERM. The filament assembly strategy involved chemically denaturing the γPFD variants and TERM in 8 M guanidinium hydrochloride and combining the individual subunits at specific molar ratios, before subsequently triggering filament assembly by dilution of the denaturant. We demonstrated that the length of γPFD-LBT and LBT-γPFD-LBT filaments could be controlled by varying the amount of TERM relative to the γPFD variants (**Figure 5**). Addition of TERM to a four-fold excess of either γPFD-LBT or LBT-γPFD-LBT produced filaments with an average length of 55 ± 12 nm and 54 ± 11 nm, respectively. These short filaments were subsequently used to fabricate REE nanoparticles, and their magnetic properties compared to REE nanoparticles were mineralized on full length LBT and LBT-γPFD-LBT filaments.

3.3 Bioengineering to Develop a Controlled Surface Layer on REE-Containing NP

Several approaches were developed to incorporate an inert shell layer of SiO2 and TiO2 on γPFD-REE nanoparticles. A variant of γPFD was cloned that contained both an LBT binding domain and a Ti binding peptide, however, this construct was unable to be recombinantly expressed. An alternative strategy involved the production of a concatenated peptide that joins the LBT domain with the Ti-binding peptide through a long linker sequence (**Figure 6**, A). Nanoparticles produced by mineralizing REE on filaments would be incubated with the peptide, which should bind the REE surface through its LBT domain and decorate the surface with the Ti binding peptide. The peptide was too large to produce using chemical synthesis, so an alternative method was developed to express the peptide recombinantly in fusion with a self-cleaving protein called an intein. The addition of dithiothreitol (DTT) was shown to trigger the cleavage and release of the LBT-Ti binding peptide (**Figure 6**, B), which could then be purified and will

now be used to decorate REE nanoparticles.

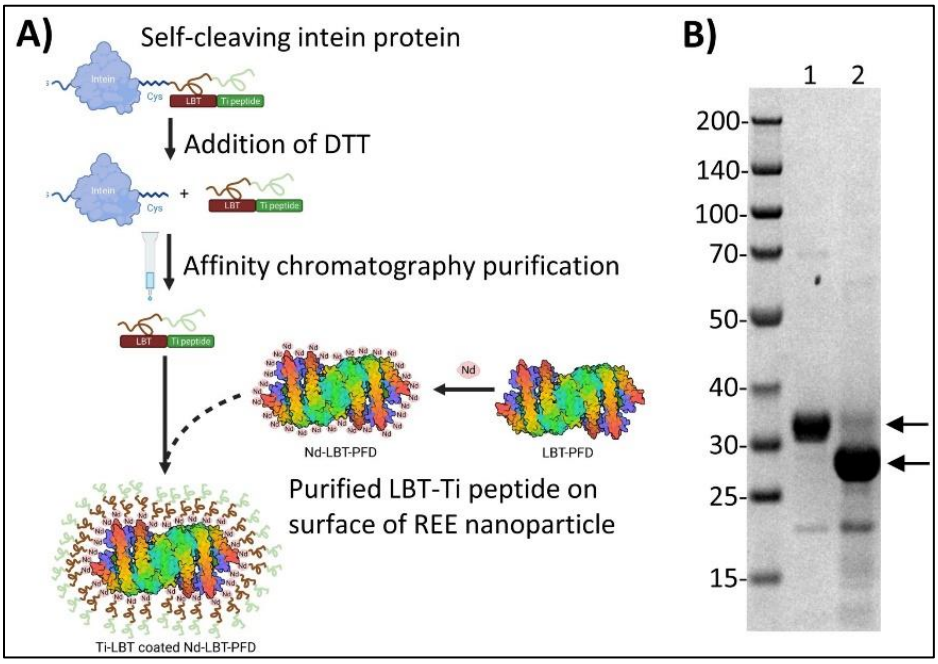

Figure 6. a) Scheme showing a self-cleaving intein protein in fusion with a sequence encoding LBT and a titanium (Ti) binding peptide, Cleavage of the LBT-Ti peptide from the intein is triggered by the addition of DTT, which will be used to coat an REE nanoparticle and mineralize a titanium shell. B) SDS-PAGE gel showing the full-length intein-LBT-Ti protein (lane 1; top arrow) and cleaving of the protein following the addition of DTT (lane 2; bottom arrow).

3.4 In-House REE-Containing Nanoparticle Characterization

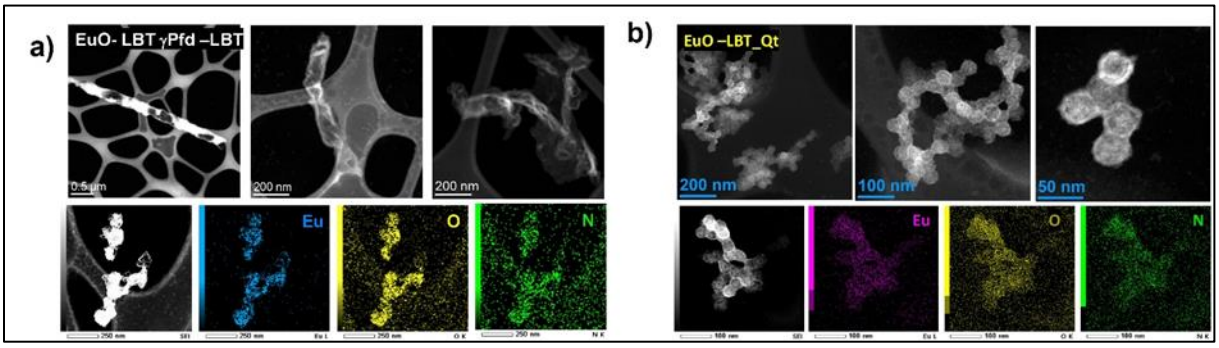

Figure 7. Representative TEM images of Eu biominerals templated on a) LBT-γPFD-LBT and b) LBT-QtEnc peptide scaffolds and ADF-STEM images with corresponding EDS element maps of Eu, O, and N

We successfully synthesized various rare earth-containing biomineral NPs using a facile biomineralization approach using genetically engineered γPFD and encapsulin, mainly focusing on the QtEnc protein from Q. thermotolerans. Proteins were functionalized with either the lanthanide binding tag (LBT) or Lanmodulin (LanM) sequences, which are known to be selective for REEs. **Figure 7** shows representative TEM images taken of Eu REEs templated on LBT-γPFD-LBT and LBT QtEnc scaffolds respectively. The images show the γPFD-templated

materials exhibiting a fused filament-like morphology, whereas the encapsulin-templated materials adopt a fused network of nanospheres. These observations provided an early confirmation that the REE biomineral morphologies are influenced by the peptide scaffolds.

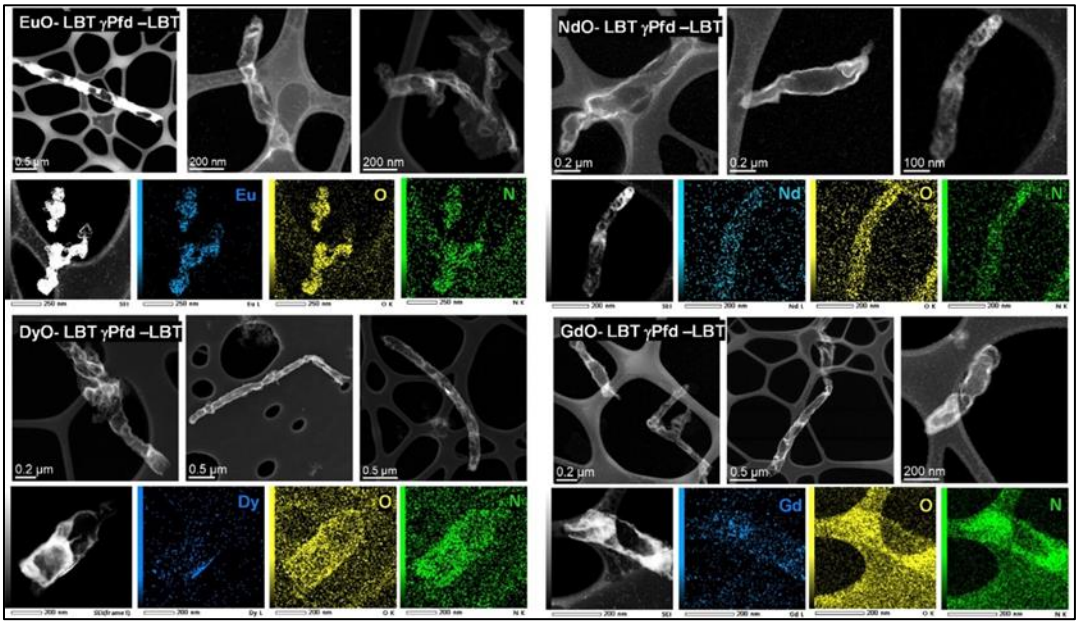

Figure 8. Representative TEM images of Eu, Nd, Dy, and Gd biominerals (from top left, clockwise) templated on LBT-γPFD-LBT peptide with ADF-STEM images and corresponding EDS element maps of REE metal species, O and N

Table 1. Approximate sizes of REE biominerals templated on LBT-γPFD-LBT peptides measured in length based on analysis of corresponding TEM images in Figure. 2 using ImageJ software

REE	SIZE (MM)
Eu LBT-γPFD-LBT	3.71 ±0.05
Gd LBT-γPFD-LBT	2.80 ± 0.01
Nd LBT-γPFD-LBT	0.55 ± 0.01
Dy LBT-γPFD-LBT	2.31± 0.02

We further examined the REE of Dy, Gd, and Nd to determine the influence of metal species on forming nanomaterials with engineered proteins. **Figure 8** shows the TEM images of different REE biominerals templated on LBT-γPFD -LBT. The images show nearly identical morphologies among the templated materials with different unit lengths (**Table 1**). The morphological effect of LBT and LanM functionalization on the protein scaffold was also investigated using Eu-based REEs. **Figure 9** shows the TEM images and the particle size distribution analysis of materials templated on QtEnc, LBT-QtEnc, and -LanM-QtEnc. The results show the REE-specific functionalization resulted in slightly larger individual diameters, but spherical morphologies were observed in all instances.

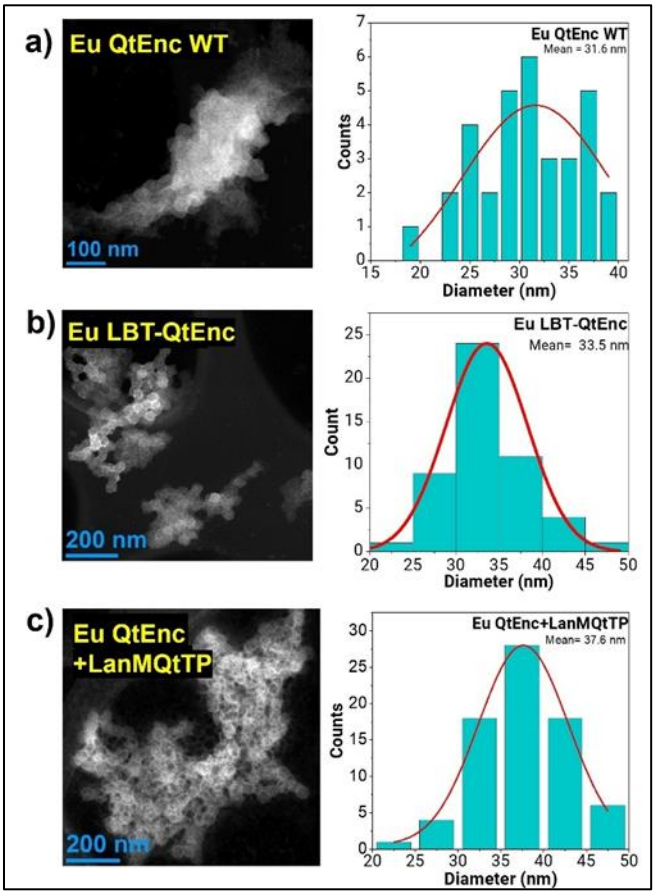

Figure 9. ADF-STEM images of Encapsulin templated Eu biominerals with corresponding particle size distribution of spherical nanoparticles

Together with the initial TEM results (**Figure 9**, A), we hypothesized the size and morphology biomineral is due to the specific REE affinity to the peptide species and the corresponding rate of nucleation and agglomeration of the individual NPs. This hypothesis is partially confirmed by HR cryo-TEM images of Dy templated on LBT-γPFD-LBT (**Figure 10**) which shows a coral-like structure composed of branching tiny filaments fused together instead of an individual peptide templated NP. This morphology has been confirmed to be a mix of nanocrystalline $Dy(NO_3)_3$ and amorphous Dy_2O_3 as confirmed with further characterization analysis (see below).

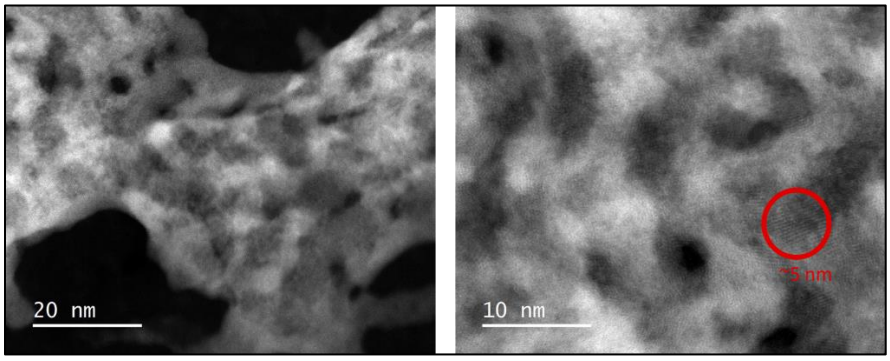

Figure 10. High-resolution Cryo-TEM images of Dy LBT-γPFD-LBT materials

4. CONTROLLED BIOENGINEERING AND CHARACTERIZATION OF SUPERPARAMAGNETIC REE-CONTAINING NANOPARTICLES

4.1 Magnetic Property Measurements of Protein-Templated and Abiotic REE-Containing Nanoparticles

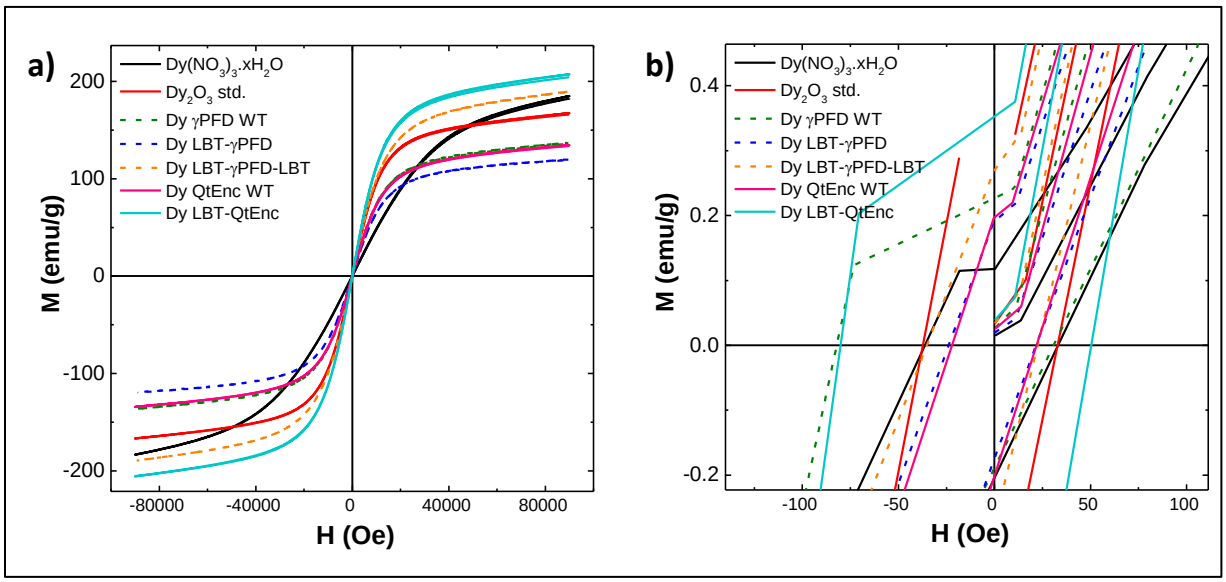

*Figure 11. Magnetic saturation curves measured at 5K of Dy biominerals templated on γPFD and QtEnc protein scaffolds, b) enlarged view of VSM plot showing remanence and coercivity values of Dy biominerals. *All data normalized by the calculated Dy wt. % analyzed using ICP-OES*

Table 2. Magnetic property data obtained at 5K for Dy biominerals templated on γPFD and encapsulin protein scaffolds

Material	M_s (emu/g)	H_c (Oe)
$Dy(NO_3)_3$. x H_2O	168	36.6
Dy_2O_3 (bulk)	192	38.4
Dy γPFD WT	137	82
Dy LBT-γPFD	120	23.6
Dy LBT-γPFD-LBT	190	34.5
Dy QtEnc WT	135	22.0
Dy LBT-QtEnc	207	80.0

Following the initial successful synthesis and TEM characterization of different REE species using the γPFD and encapsuling, we turned our Dy-based materials given their enhanced magnetic properties compared with Eu, Nd, and Gd-based materials. This allows for an analysis of how different protein scaffolds and peptide functionalization can specifically influence species to study the effect of different peptide scaffolds on the magnetic behavior of Dy-based materials.

Magnetization curse obtained at 5K (**Figure 11** A & B) illustrate that both γPFD and QtEnc

templated materials generally outperform bulk $Dy(NO_3)_3.xH_2O$ and Dy_2O_3 materials, showcasing the important role biotic-abiotic interactions can be used to modulate and improve upon magnetic properties. Dy-LBT QtEnc sample with the highest saturation magnetization (Ms) at 207 emu/g, followed closely by LBT-γPFD-LBT templated Dy at 190 emu/g. Importantly, both instances showcase the importance of LBT on the resulting magnetic properties, which exhibit improved properties of WT-templated materials. This phenomenon likely arises from the peptide's high affinity for Dy during the mineralization process. Our findings further demonstrate that coercivity (Hc) can be affected by the type of scaffold implemented for the Dy-based materials. For example, Dy QtEnc WT (22.0 Oe) vs. Dy γPFD WT (82.0 Oe) showcases the template morphology (cages vs filaments) can be important, Moreover, LBT functionalized can be implemented to further modulate coercivity. In the γPFD templated materials, LBT functionalization lowers Hc values vs. the γPFD WT. Conversely, LBT-QtEnc material exhibits a higher Hc value vs. the QtEnc WT. Overall these results demonstrate that the magnetic properties of Dy REEs can be modulated with different scaffolds and LBT functionalization. Additional characterization work is presently underway (with results to date summarized below) to investigate the impact of the biotic-abiotic interactions that may influence overall magnetic behavior.

4.2 Multi-Element REE Nanoparticles Templated on Engineered Protein Scaffolds

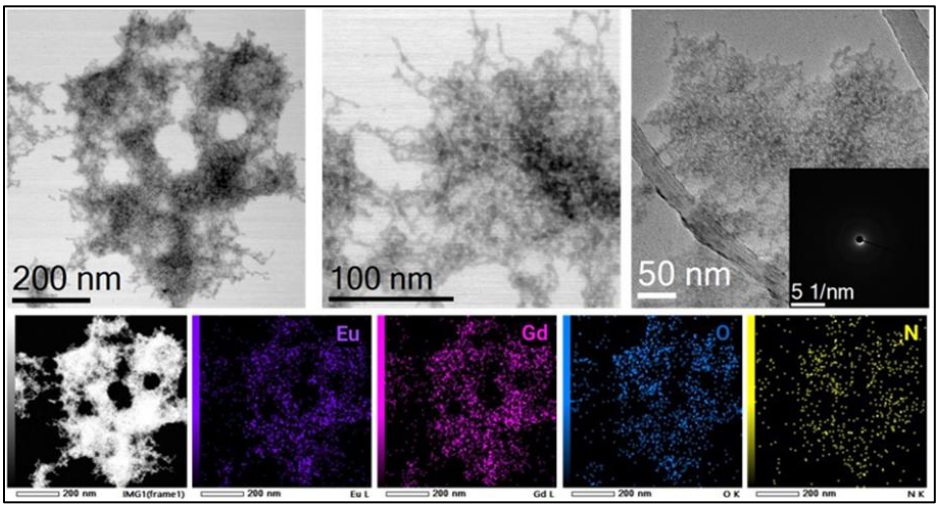

Figure 12. (Top row) TEM images of Gd:Eu (50:50) LBT-γPFD with SAED image (inset). ADF-STEM image with corresponding EDX element maps of Gd, Eu, O, and N

Apart from monometallic REEs, we confirmed that the original synthesis protocol can be used to synthesize bimetallic REEs. **Figure 12** shows the representative TEM images of Gd:Eu templated on LBT-γPFD. The results show the uniform distribution of both metal species throughout the protein scaffolds, and exhibiting the morphologies seen previously in the monometallic REEs. To investigate the effect of two REE species in a protein system towards magnetic behavior, we prepared Gd:Dy biominerals in varying weight percent ratios. This particular combination is an ideal choice for studying magnetic behavior due to their reported studies as T1 and T2 contrast agents for magnetic resonance imaging (MRI) respectively.

For the synthesis experiment, we chose to use LBT-γPFD-LBT protein as the scaffold based on our initial γPFD size control experiment. The volume of Dy-precursor added was kept constant with the Gd changed accordingly to achieve the desired ratio. ICP-OES analysis of the lyophilized Gd:Dy biominerals confirms that the weight percent ratios were close to the volume ratios used during synthesis. The total metal concentration was used to normalize the magnetization data due to the magnetic nature of both species. Magnetization data (**Table 3**) show at 5K that introducing £ 30% of Gd Wt.% in the same system as Dy resulted in an ~8-10% increase in saturated magnetization (emu/g) and a ~50 % increase in coercivity (Oe) in comparison to the control Dy LBT-γPFD-LBT material. At a 50:50 ratio, the saturated magnetization and coercivity decrease to their lowest values at 177 emu/g and 25 Oe. At higher Gd concentrations (70<x<95%), the coercivity values remained between 31-34 Oe. However, the saturated magnetization decreased from 202 - 180 emu/g as the Gd concentration increased to 95 %. The trends above show that at low concentrations Gd can increase both saturated magnetization and coercivity in a Gd:Dy system. We hypothesized that the enhancement could be due to the Gd-phase acting as an interstitial impurity. In this scenario, the Gd atoms could act as pinning points for the magnetic moment by affecting the electron spin of the neighbouring Dy-atoms. Further characterization experiments are being planned to investigate the electronic interaction of the Gd and Dy atoms in relation to their magnetic properties.

Table 3. Magnetization data for Gd:Dy biominerals templated on using uncapped LBT-γPFD-LBT obtained at 5K

Material	M_s (emu/g)	H_c (Oe)
$Dy(NO_3)_3$. x H_2O	168	36.6
Dy_2O_3 (bulk)	192	38.4
Dy γPFD WT	137	82
Dy LBT-γPFD	120	23.6
Dy LBT-γPFD-LBT	190	34.5
Dy QtEnc WT	135	22.0
Dy LBT-QtEnc	207	80.0

*Data is normalized using the total weight percent of REE in each material as measured by ICP-OES

To investigate the ability of using engineered proteins to create non-magnetic capping shells onto the REEs, we investigated a TiO_2 as shell material on Dy REEs using the encapuslin variant QtTi. Based off QtEnc, QtTi possesses exterior facing Ti-binding tags on the nanocage structure, guiding TiO_2 shell formation outside the protein cage. via biomineralization. By modifying the amount of Ti(IV) bis(ammonium lactate)dihydroxide during synthesis, the potential thickness of the TiO_2 shell may be controlled. XPS analysis (**Figure 13**) of the composite nanostructures excluding the Ti 0%-Dy QtTi1 material shows all the Ti-species present adopt a +4 oxidation state +4-oxidation similar positions of the Ti 2p3/2 (458.5 eV) and Ti 2p1/2 (464.3 eV) peaks. The fitted O1s XPS spectra also show peaks at 529.9 eV consistent with lattice oxide (O-M) confirming the presence of TiO_2 on the surface. Analysis of the Dy 3d5/2 peaks in all the material also shows similar positions at ~1296 eV indicating a +3 oxidation state with and

without TiO_2 present.

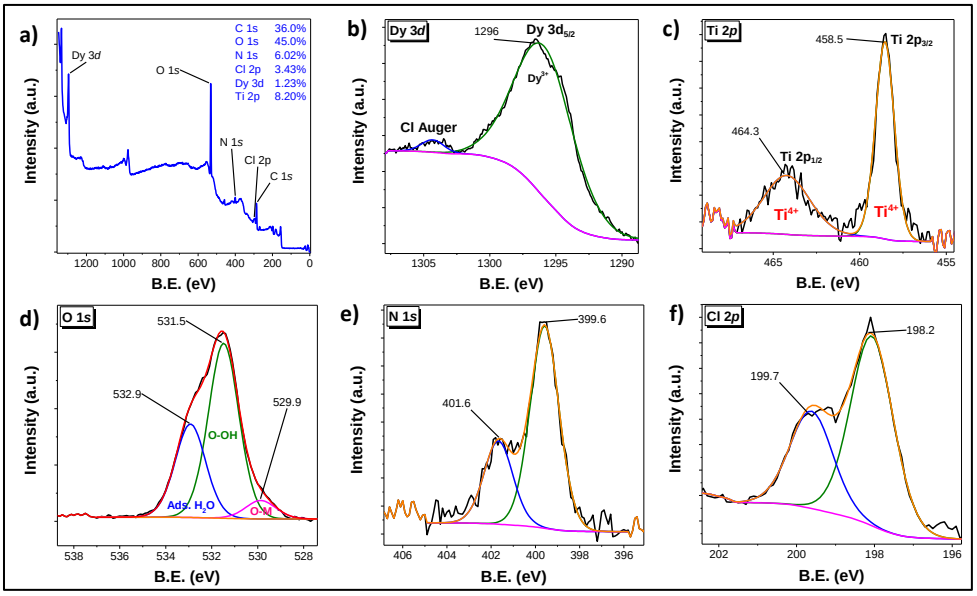

Figure 13. Representative XPS data for Ti 9.54%-Dy QtTi1 material, a) Survey XPS with calculated surface atomic %, deconvoluted high-resolution XPS scans of b) Dy 3d, c) Ti 2p, d) O 1s, e) N 1s, and f) Cl 2p region

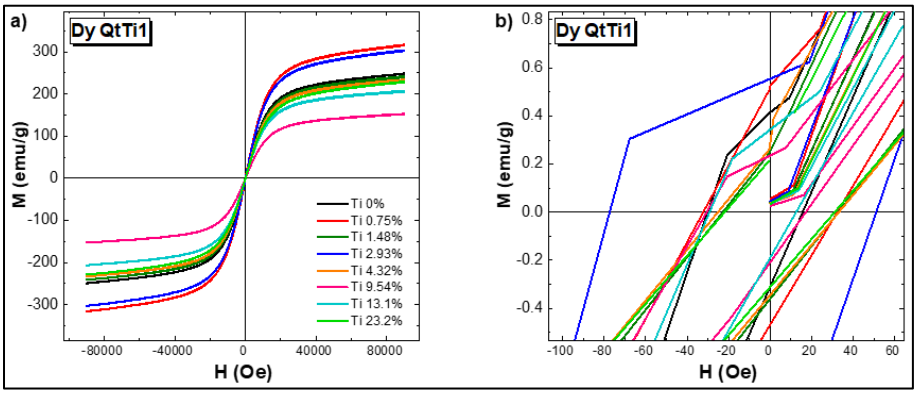

*Figure 14. a) Magnetisation curves obtained at 5K of Dy QtTi materials with different Ti wt.% concentrations b) Enlarged view plot showing remanence and coercivity values. * Data is normalized using calculated Dy wt.% measured from ICP-OES*

Magnetization curves (**Figure 14**) show that introducing TiO_2 as a shell material generally have a positive effect on the magnetic performance when compared to the Dy-only materials at low Ti concentrations. At higher concentrations, there is a diminishing return toward performance, suggesting that increased TiO_2 disrupts the ordering of the magnetic moment of the Dy phase within the material. We are currently planning to conduct further characterization experiments to study the crystal structure of the composite material. Experiments involving XAS and PDF would be instrumental in determining the effect of the Ti-species on the electronic structure and identifying the bulk phases.

4.3 Size-Constrained REE-Containing Nanoparticles Engineered Protein

Templates

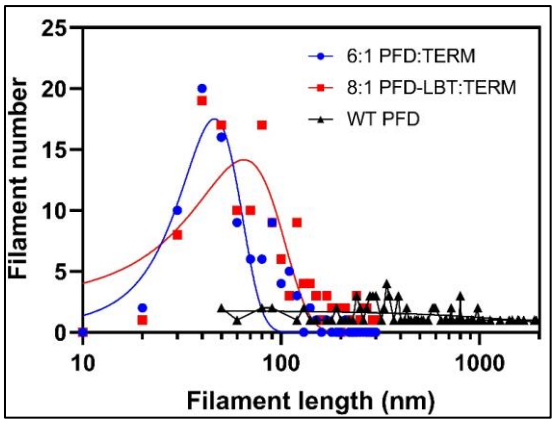

Figure 15. Size distribution of filament lengths of TERM capped γPFD compared to uncapped wild-type PFD

To explore the effect of size on magnetic behavior, we conducted synthesis experiments using TERM as a capping agent for controlling the filament length of γPFD peptides expressed by the E.Coli host. By modifying the molar ratio of the peptide against TERM, we were able to control the strand length and achieve a relatively uniform size distribution (**Figure 15**). For initial synthetic testing and downstream magnetic properties measurements, we chose to experiment with γPFD (6:1) TERM capped system. The 6:1 ratio yields γPFD filaments with a mean strand length of 40 nm. In comparison, the unconstrained γPFD exhibits randomized distributions of filaments that are 20-4000 nm in length.

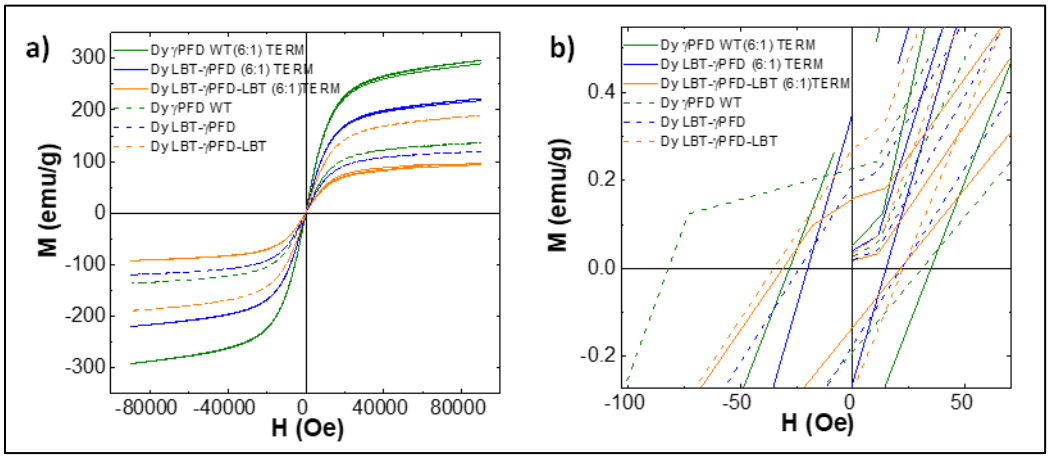

Figure 16. a) Magnetization curves for Dy biominerals templated on TERM-capped γPFD compared against unmodified γPFD, b) enlarged view showcasing hysteresis properties. All plots are measured at 5K and normalized using the Dy weight obtained from ICP-OES measurements

Table 4. Magnetic property data for Dy biominerals templated using TERM capped and uncapped γPFD variants measured at 5 K compared against Dy nitrate and oxide reference materials

Material	M_s (emu/g)	H_c (Oe)
Material	M_s (emu.g^{-1})	H_c (Oe)
$Dy(NO_3)_3$. x H_2O	168	36.6
Dy_2O_3 standard	192	38.4
Dy γPFD WT	137	82
Dy LBT γPFD	120	23.6
Dy LBT γPFD LBT	190	34.5
Dy γPFD WT (6:1) TERM	296	28.1

Magnetic property data (**Figure 16**) show the biominerals templated on the TERM-capped materials outperforming the uncapped variants in terms of saturated magnetization (Ms) values. Interestingly, the magnetic performance trend does not follow the order observed in the uncapped materials (**Table 4**). The results show the Dy γPFD WT (6:1) TERM having the highest Ms value (296 emu/g) compared to other TERM-capped LBT-functionalized variants. This result is a contrast to the uncapped materials where the Dy LBT γPFD LBT material has the highest Ms (190 emu/g). The results also show the TERM-capped materials with lower coercivity values compared to the uncapped variants. In both material sets, the single fused LBT variant exhibits the lowest Hc value. The decrease is most significant in the Dy γPFD WT TERM material. The influence of γPFD filament length, the addition of LBT functionality, and resulting magnetic properties are presently under additional investigation.

5. ABIOTIC REE-CONTAINING NP SYNTHESIS FOR BENCHMARKING BIOGENIC MATERIALS

5.1 Abiotic REE-Containing Nanoparticle Synthesis: REE, Mn, and Fe-Containing Materials

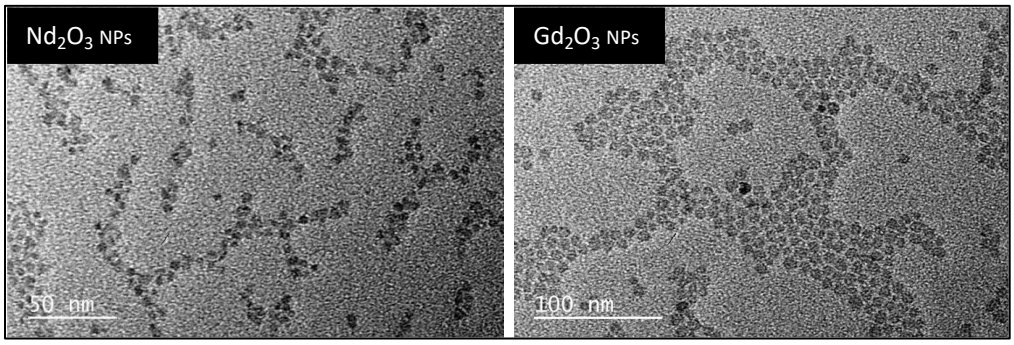

Figure 17. Representative TEM images of Nd2O3 and Gd2O3 NPs synthesized using abiotic synthesis protocol

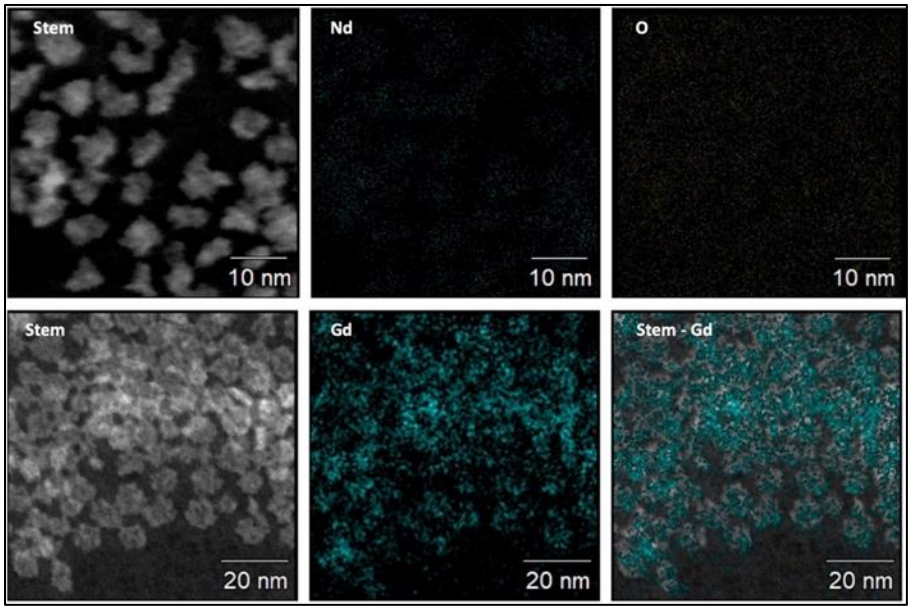

Figure 18. ADF-STEM images with corresponding EDX element maps of Nd, Gd, and O for Nd2O3 (top row) and Gd2O3 NPs (bottom row)

We successfully synthesized REE (Nd and Gd) containing NPs via abiotic synthesis protocol for magnetic performance comparison against the templated γPFD and encapsulin counterparts (**Figure 17**). The synthesis protocol involves the mixing of REE-based acetylacetonate precursors in a mixture of benzyl ether, oleic acid, and oleylamine. The reaction produces a REE-oleate precursor which is reacted slowly with oleyl alcohol to remove excess oleic acid for 24 hours before recovery by centrifugation. TEM analysis reveals the Nd_2O_3 and Gd_2O_3 exhibiting spherical morphologies with average diameters of 5.6 ± 0.9 nm and 8.5 ± 0.9 nm respectively. EDX element mapping of the REE-containing NPs shows the uniform distribution

of the corresponding metal species alongside oxygen in the nanostructures, confirming the successful synthesis of metal oxide phases (**Figure 18**). Similar synthetic methods are presently being adapted for Dy_2O_3.

6. ATOMIC-SCALE MATERIALS CHARACTERIZATION TO ESTABLISH BIOGENIC STRUCTURE/FUNCTION RELATIONSHIPS

6.1 Liquid Cell TEM to Observe Real-Time Nucleation and Growth Mechanisms

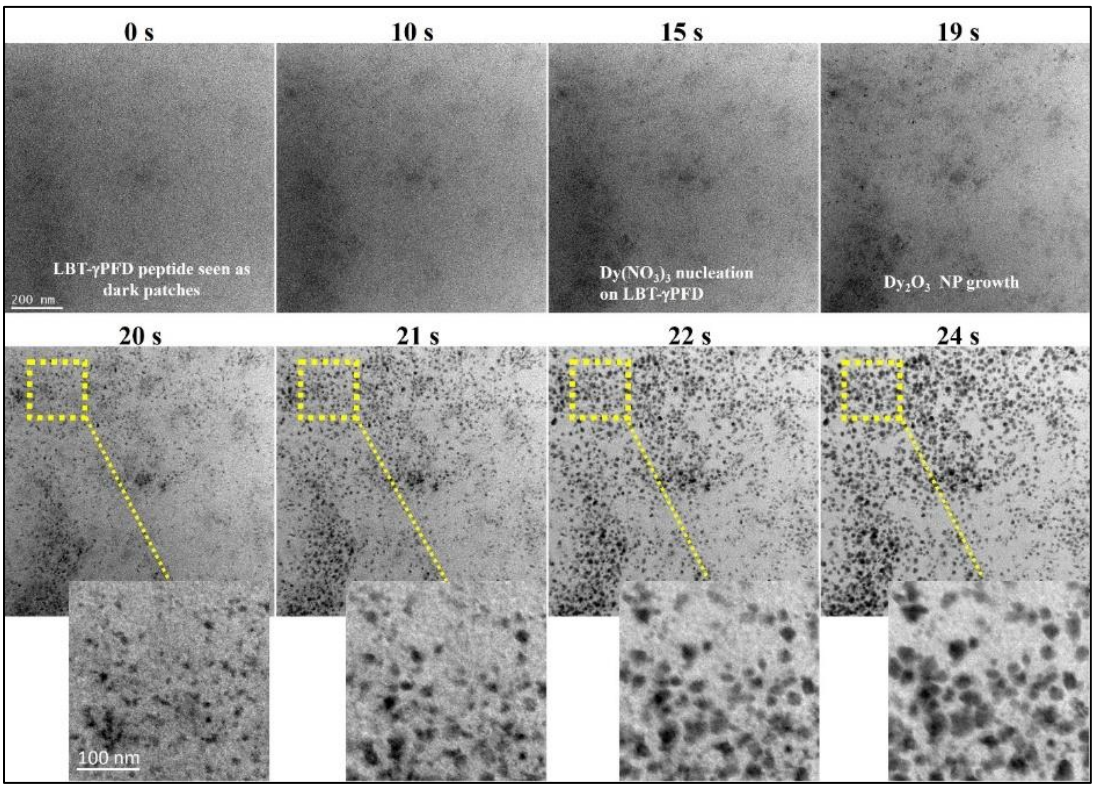

*Figure 19. Time-resolved liquid-cell TEM images of Dy LBT-γPFD biomineral formation in 0.1 M Tris-HCl solution (pH 7.5) observed over a period of 24 seconds. * Each image still is an average of 10 frames taken during the measurement*

Liquid cell TEM experiments were conducted to further investigate the crystal growth mechanism in the Dy biomineral templated on LBT-γPFD protein. Materials for the liquid cell TEM experiment were chosen based on the precipitation behaviour in normal lab conditions. Among studied materials, the Dy LBT-γPFD exhibited the fastest onset of colloidal NP formation within 8-10 minutes making it suitable for in-situ imaging. To minimize the effect of rapid agglomeration and damage to the TEM cell, the Dy(NO3)3.xH2O precursor and LBT-γPFD solutions were diluted to a 1:1 ratio at a concentration of 0.41mg/ml. The flow of the precursor and protein solutions was also kept very low at 1µl/min. Image acquisition was focused on areas with dark patches that belong to the γPFD protein to capture the nucleation of templated Dy biomineral NPs. Time-lapse acquisition was performed to create a series of stills showing the evolution of crystal growth. The results confirm the LBT-γPFD protein behaving as nucleation sites for the solvated Dy precursor as evidenced by the evolution of NPs forming around the dark patches corresponding to the proteins (**Figure 19**). The resulting Dy initially

forms individual NPs before agglomerating to form larger crystals as time increases. The interpretation of these results is ongoing; however, the morphology of these materials clearly differs from the TEM results seen post-synthesis for all bioengineered REEs to date. This suggests that we are only observing the starting nucleation and growth of the materials within the liquid cell, and/or electron beam damage effects are leading to changes to REE morphology.

6.2 XAS for Probing the Local Structure of Biogenic REE-Containing Nanoparticles

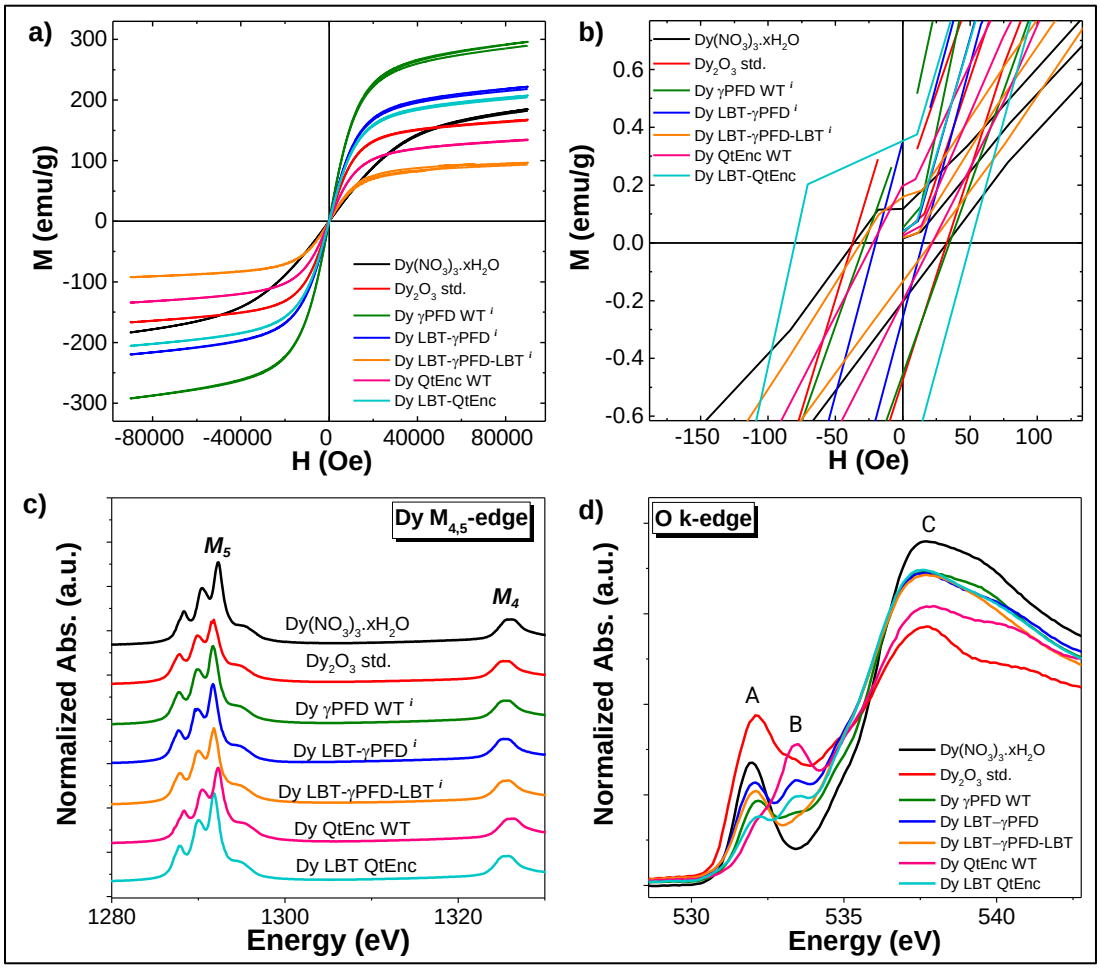

*Figure 20. Magnetization plots obtained at 5K of Dy REE templated on TERM-capped γPFD and encapsulin proteins vs. Dy2O3 and Dy(NO3)3.xH2O references, b) enlarged view showing remanence and coercivity values, c) Corresponding Dy M 4, 5-edge XAS plots, and d) O K-edge XAS plots. * i: γPFD materials are TERM-capped at a 6:1 molar ratio to achieve an average filament length of 40nm.*

Based on the excellent magnetic performance of the TERM-capped γPFD templated Dy biominerals, we conducted X-ray absorption spectroscopy (XAS) measurements at the Dy M 4, 5 and O K-edge to characterize the contribution of the protein scaffold towards the electronic structure and relationship to magnetic performance. These results were also compared against the encapsulin-templated materials to verify any similar activity descriptors. Figure. 20 c shows all the Dy-biominerals exhibiting similar peak energy positions as the Dy(NO3)3.xH2O and Dy2O3

references, which indicate a similar Dy oxidation state of +3 in all materials. We chose to turn our attention instead to the O K-edge XAS measurements (**Figure 20**, D) of the Dy-biominerals. The O K-edge XAS profiles show a correlation between the intensity of the peak profile at ~537.5 ± 0.3 eV present in all materials corresponding to the O 1s → Dy 5d transition, where this intensity of this feature can be related to the covalency of the metal-oxygen bond. It can be hypothesized that the strength of the bond covalency affects the number of unpaired electrons shared between the Dy and O atoms which can be related to the magnetic strength of the Dy REEs. Further experimentation is ongoing to verify this hypothesis.

6.3 Atomic PDF Analysis Coupled to RMC Structure Modeling for Constructing REE-Containing Nanoparticle Structure Models

Different crystallographic models were tested to fit the obtained PDF data for REE synthesized in Month 1-4. The promising and best fit was achieved with Gd nitrate pentahydrate (triclinic P-1. SG no. 2). Lattice parameters, angle, atomic coordinates, and RE occupancies were refined in a controlled manner using PDFgui software. The modelled fit matches well with the experimental data, as shown in (**Figure 21**). Obtained fit parameters (**Table 5**) and a few exemplary fits are shown below. These models suggest that the crystalline components of the REE are nitrates in nature, as shown by HR-TEM, which will be overrepresented in the PDF fits. PDF data (**Table 5**) was also obtained for Dy-containing NPs templated on γPFD and encapsulin proteins to determine the crystalline phases present following biomineralization. A systematic study on Dy-based materials was recently performed at ESRF, with the resulting first shown in (**Figure 21**). The crystallographic PDF fits reveal the materials also contain nitrate crystallites, as evidenced by the quality of fits in **Figure 19** and **Table 6**. HR-TEM showcases that amorphous regions of Dy_2O_3 likely exist, which will be modelled in future efforts using reverse Monte Carlo (RMC) simulations.

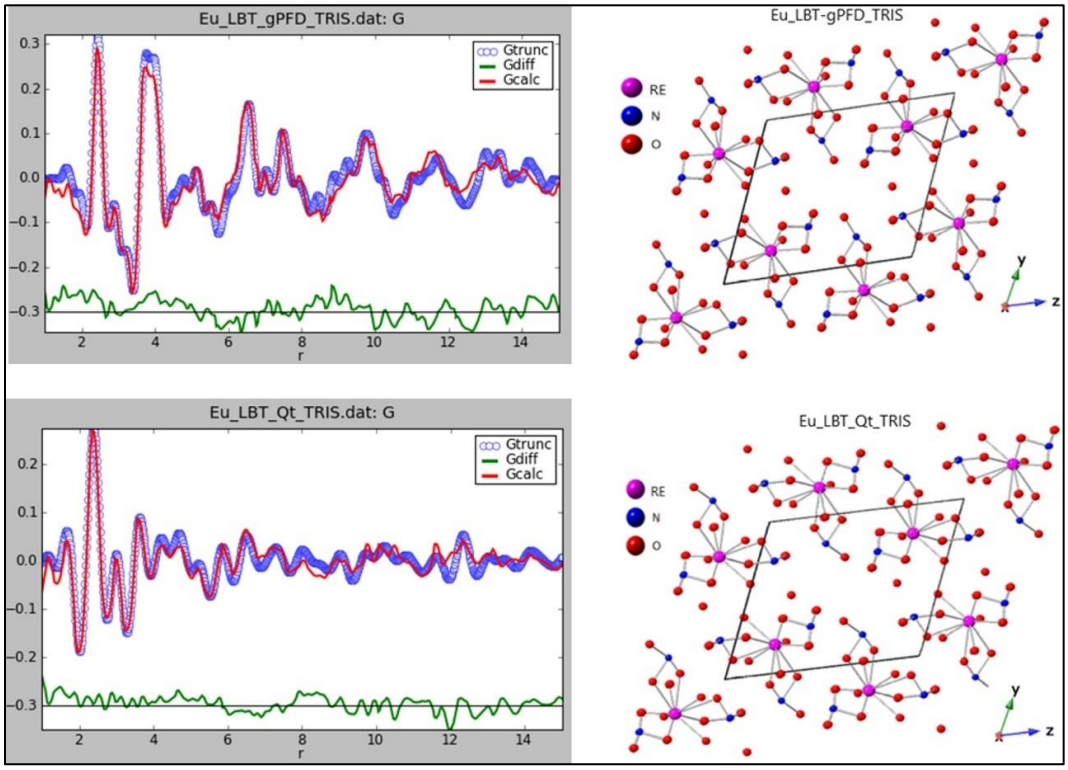

Figure 21. Representative data fitting for Eu-biominerals templated on LBT-γPFD and LBT-Qt done in PDFgui. Experimental data (blue symbol) fitted data (red line) and the difference between experimental and fitted data (green line) are shown (left panel). The right panel shows the triclinic structure and atomic distribution of modelled fit (plotted using Crystal Maker). * TRIS annotation refers to the Tris-HCl buffer system that was used to synthesize the biomineral.

Table 5. The average fit parameters for biomineral templates were obtained from PDF fit using the triclinic (P-1) space group. The initial model for the fitting was taken from Gadolinium nitrate pentahydrate (as mentioned in the menu of the table)

Material Name	a	b	c	α	β	γ	Rare Earth Occupancy
$Gd(NO_3)_3(H_2O)_4].H_2O$	6.69	9.59	10.6	63.7	84.7	76.2	
Eu LBT-γPFD	6.36	9.99	11.0	66.1	83.3	76.8	0.190
Eu LBT-Qt	6.62	9.60	10.1	68.2	81.1	67.3	0.217
Eu:Gd (50:50) LBT Qt	6.34	9.87	11.0	66.5	83.8	76.5	0.215
Eu:Nd (50:50) LBT-Qt	6.33	9.98	11.1	66.1	83.4	76.6	0.229
Eu+Nd_LBT_Qt_b	6.37	9.98	11.0	66.2	83.6	76.5	0.202
Gd LBT-γPFD	6.36	9.89	11.0	66.3	84.1	76.6	0.197
Gd LBT-Qt	6.36	10.0	11.2	66.0	84.6	76.8	0.173
Gd:Nd (50:50) LBT Qt	6.33	9.94	11.0	66.0	83.5	76.4	0.189
Dy LBT-Qt	6.32	9.98	11.1	65.9	84.7	77.2	0.210

Table 6. The average fit parameters for biomineral templates obtained from PDF fit using the triclinic (P-1) space group and cubic (Ia-3) space group

Material Name	a	b	c	α	β	γ	Rare Earth Occupancy
$Gd(NO_3)_3(H_2O)_4].H_2O$	6.69	9.59	10.6	63.7	84.7	76.2	
Dy γPFD WT	6.24	9.75	10.8	66.2	83.6	76.7	0.142
Dy LBT-γPFD	6.26	9.79	10.8	66.3	83.8	76.5	0.122
Dy LBT-γPFD-LBT	6.25	9.76	10.8	66.2	83.7	76.6	0.134
Dy LBT-Qt	6.29	9.79	10.8	66.2	83.7	76.2	0.133
Dy QtEnc WT	6.29	9.81	10.8	66.3	83.8	76.2	0.139
Cubic (Ia-3) SG. 206							
Dy_2O_3 reference	10.7						

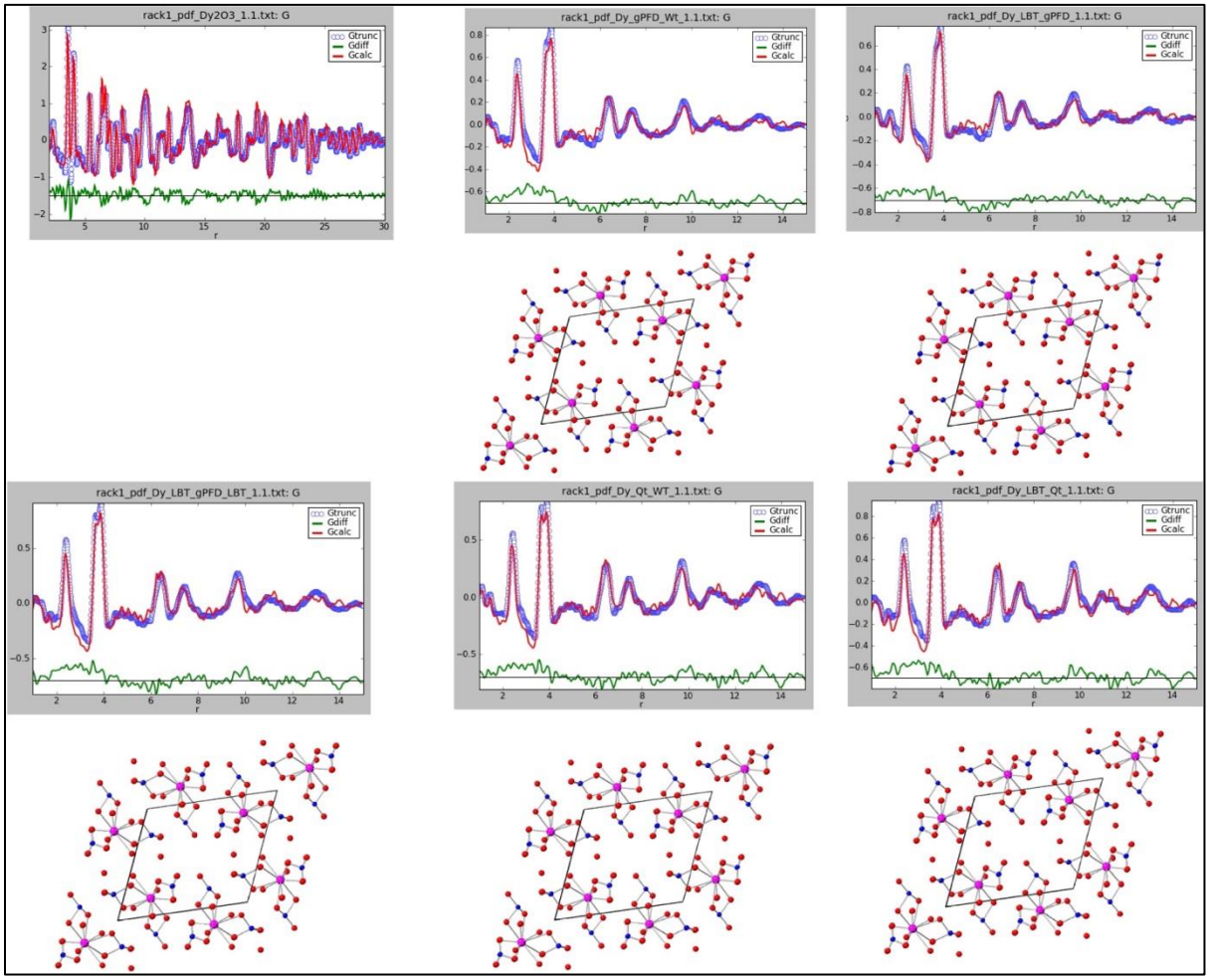

Figure 22. Data fitting of Dy biominerals templated on γPFD and QtEnc variants with Dy2O3 reference done on PDFgui. Experimental data (blue symbol) fitted data (red line) and the difference between experimental and fitted data (green line) are shown (left panel). The right panel shows the triclinic structure and atomic distribution of modelled fit (plotted using Crystal Maker).

7. SYNTHETIC METHOD OPTIMIZATION OF THE TEMPLATE REE-CONTAINING NPS\

7.1 Optimized REE NP Characterization

The synthetic method for templated REE-containing NPs was refined to optimize morphology and magnetic properties. The $Dy(NO_3)_2$ precursor concentration was reduced by ×30, and the buffer solution volume was increased to prevent nucleation and minimize unreacted $Dy(NO_3)_2$ on the genetically engineered γPFD protein. Figure 23 illustrates a distinct thin wiring structure of γPFD-LBT and LBT-γPFD-LBT resembling the original protein structure (**Figure 4**), in contrast to the previously observed fused network (**Figure 12**). This optimized synthesis method significantly reduces agglomeration. Additionally, EDS mapping reveals an O: Dy peak intensity ratio of 3:2 and a reduced N peak intensity, indicating that the material is predominantly Dy_2O_3 rather than $Dy(NO_3)_2$.

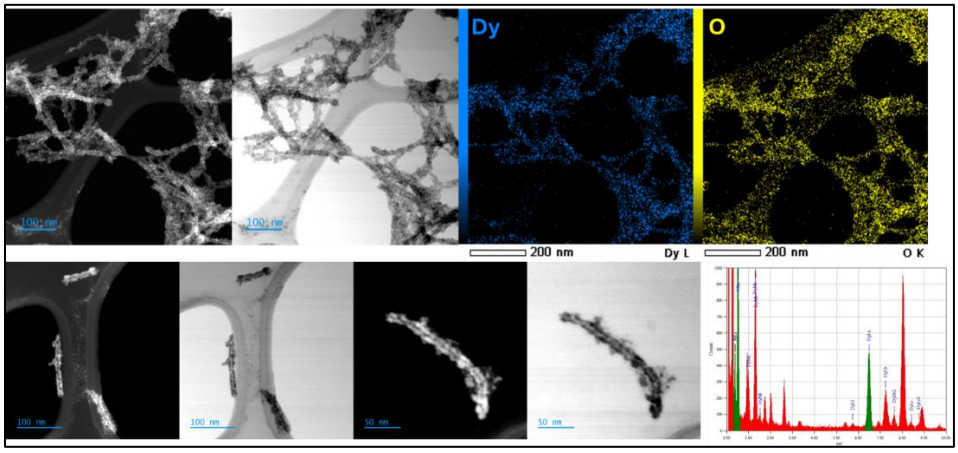

Figure 23. Representative TEM images of Dy biominerals templated on γPFD-LBT peptide with ADF-STEM images and corresponding EDS element maps (Dy and O) and spectrum.

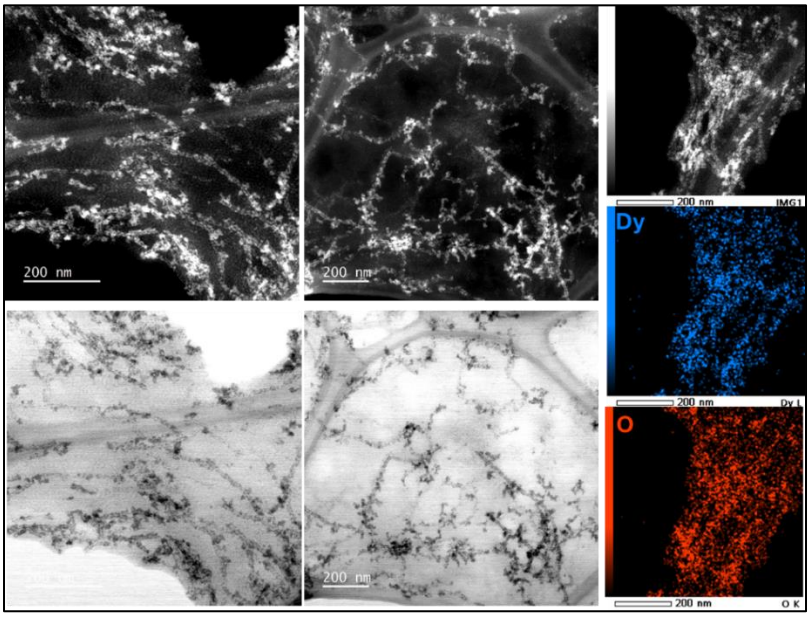

Figure 24. Representative TEM images of Dy biominerals templated on LBT-γPFD-LBT peptide with ADF-STEM images and corresponding EDS element maps (Dy and O)

The generality of the synthetic method for templated REE-containing nanoparticles (NPs) was further evaluated using capped proteins with 4:1 and 6:1 molar ratios of TERM. **Figure 25** and **Figure 26** demonstrate that the capped proteins exhibit distinctly shortened wire structures, similar to the bare capped protein shown in **Figure 5**. These results confirm the general applicability of the optimized synthetic method across various proteins, including modified ones.

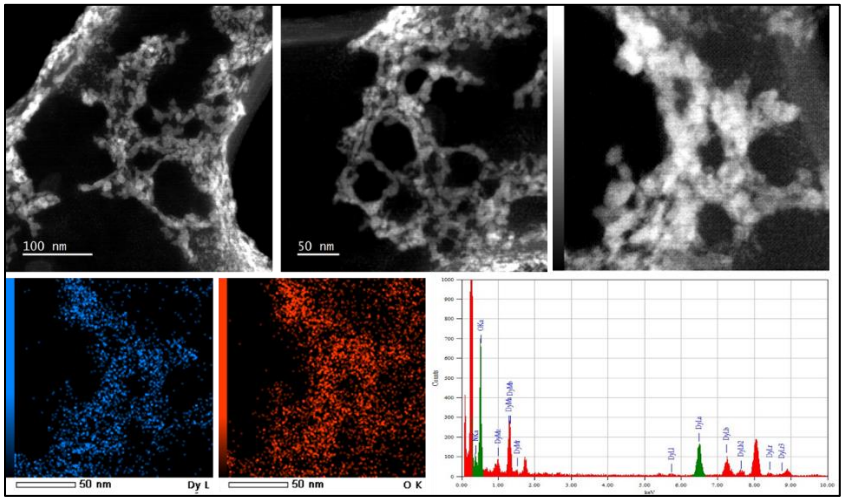

Figure 25. Representative TEM images of Dy biominerals templated on a 4:1 molar ratio γPFD-LBT:TERM peptide with ADF-STEM images and corresponding EDS element maps (Dy and O)

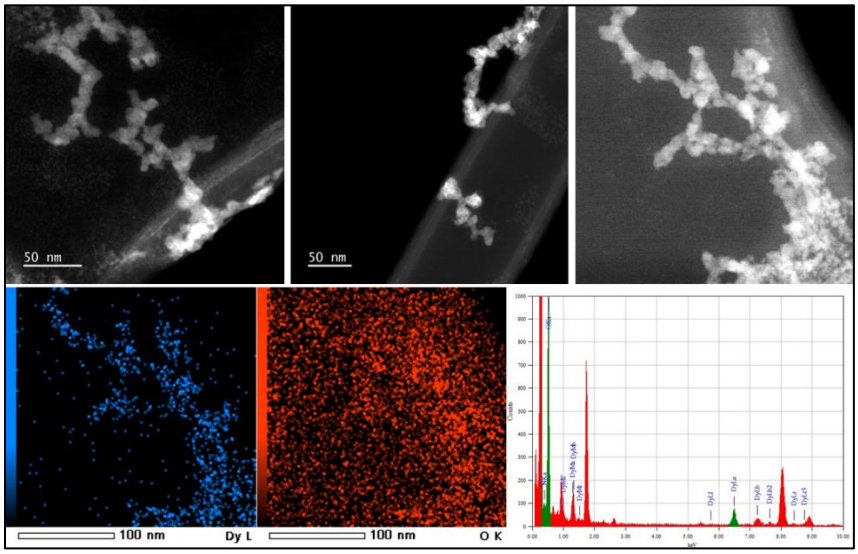

Figure 26. Representative TEM images of Dy biominerals templated on 6:1 molar ratio γPFD-LBT:TERM peptide with ADF-STEM images and corresponding EDS element maps (Dy and O)

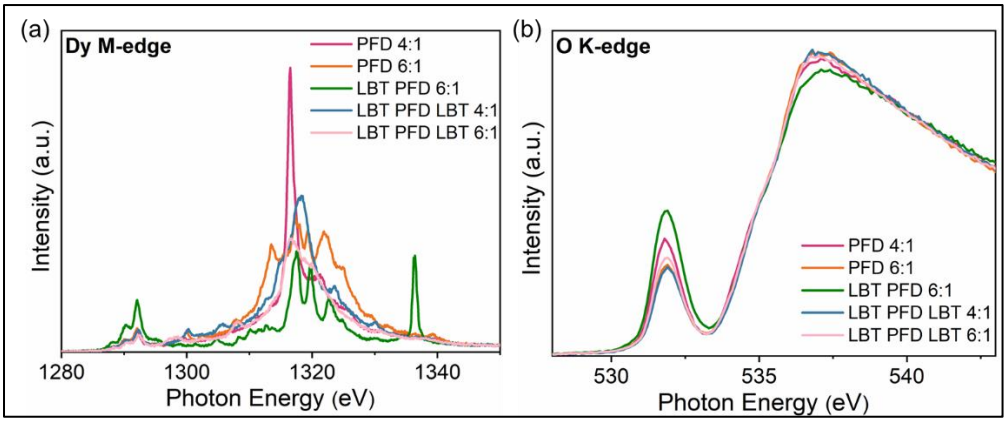

Figure 27. Dy M4,5-edge XAS plots, and d) O K-edge XAS plots. of the γPFD-LBT materials TERM-capped at a 4:1 and 6:1 molar ratio.

X-ray absorption spectroscopy (XAS) measurements at the Dy M4,5 and O K-edge were performed to elucidate the contribution of the protein scaffold to the electronic structure and its relationship to magnetic performance. **Figure 27** shows that all Dy-biominerals exhibit distinct electronic structures at the Dy M4,5 edges, indicating that filament length may significantly affect the electronic structure of the Dy metal. Further interpretation of these data is needed to correlate them with the magnetic properties.

Magnetic property data (**Figure 28** and **Table 7**) indicate that REE-containing NPs synthesized using the optimized method exhibit superior saturated magnetization (Ms) values compared to previous results. Specifically, the Dy γPFD WT synthesized with the new method achieves the highest Ms value of 275 emu/g at 5 K, outperforming previous samples and other LBT-functionalized variants. The Dy γPFD WT materials also display a coercivity value of 27.2, comparable to the LBT variants. Additionally, the Dy γPFD WT demonstrates the highest Ms

value of 37 emu/g at 300 K. The TERM-capped γPFD protein series have also been synthesized and submitted for magnetic property characterization.

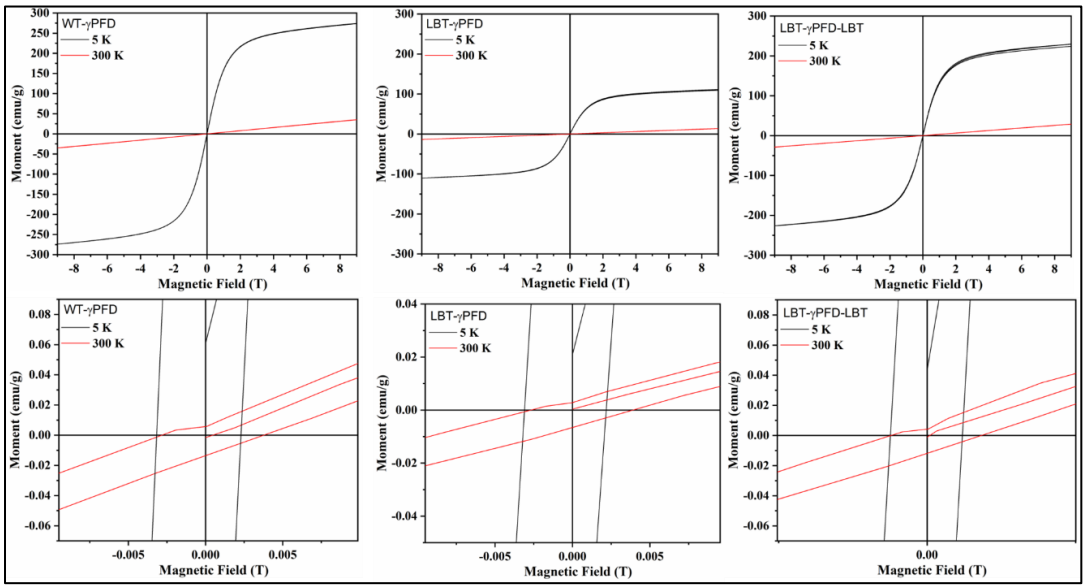

Figure 28. Magnetization plots obtained at 5K and 300K of Dy REE templated on TERM-capped γPFD, LBT-γPFD, and LBT- γPFD-LBT, b) enlarged view showing remanence and coercivity values

Table 7. Magnetization plots obtained at 5K and 300K of Dy REE templated on TERM-capped γPFD and encapsulin proteins vs. Dy2O3 and Dy(NO3)3.xH2O references and the previous results of the same sample series

Material	M_s (emu/g)	H_c (Oe)
$Dy(NO_3)_3$. x H_2O	168	36.6
Dy_2O_3 (bulk)	192	38.4
Dy γPFD WT	137	82
Dy LBT-γPFD	120	23.6
Dy LBT-γPFD-LBT	190	34.5
Dy γPFD WT_new_5k	275	27.2
Dy LBT-γPFD_new_5k	111	26.3
Dy LBT-γPFD-LBT_new_5k	230	24.1
Dy γPFD WT_new_300k	37	33.0
Dy LBT-γPFD_new_300k	15	34.0
Dy LBT-γPFD-LBT_new_300k	28	32.1

8. CONCLUSION

This project has successfully demonstrated the capability of using engineered proteins as templates for synthesizing magnetically active rare earth element (REE) nanoparticles, with a particular focus on Dy-based materials. Utilizing filamentous γ-prefoldin (γPFD) and encapsulin protein cages, both in their wild-type forms and functionalized with REE-binding motifs, we have made significant advancements in achieving well-structured nanoparticles with enhanced magnetic properties.

- We developed an optimized synthetic method that significantly improved the morphology and reduced agglomeration of Dy-containing nanoparticles. The Dy γPFD WT variant achieved exceptional saturation magnetization (Ms) values of 275 emu/g at 5 K and 37 emu/g at 300 K. The generality of the optimized synthetic method was confirmed by applying the method to varied protein templates, and the synthetic method shows applicability across various protein templates, including modified ones.

- Regarding the magnetic properties, the optimized Dy γPFD WT materials exhibited a coercivity (Hc) of 27.2 Oe, comparable to other LBT-functionalized variants, highlighting the effectiveness of our synthetic approach. Further, the TERM-capped γPFD variants showed exceptional magnetic performance, with the TERM-capped Dy γPFD WT (6:1) achieving the highest Ms value of 296 emu/g at 5 K. The above finding reveals the importance of precise control over filament length and morphology in enhancing magnetic properties. Comparative analysis showed that the magnetic performance of protein-templated Dy materials generally outperformed bulk $Dy(NO_3)_3 \cdot xH_2O$ and Dy_2O_3 materials, emphasizing the potential of biotic-abiotic interactions in enhancing magnetic properties.

- We employed advanced characterization techniques, including high-resolution cryo-EM, XAS, and PDF, to gain detailed insights into the structure and properties of the synthesized materials. XAS measurements at the Dy M 4, 5 and O K-edge revealed that filament length significantly affects the electronic structure of the Dy metal, which in turn influences magnetic performance. Further, the correlation between the covalency of the metal-oxygen bond and saturation magnetization, as revealed by XAS, suggests that a stronger covalent bond is associated with higher magnetic performance. This correlation between electronic structure and magnetic properties provides a deeper understanding of the material's behavior.

- The project highlighted the critical role of biotic-abiotic interactions in modulating the properties of REE-based nanomaterials. TERM-capped γPFD variants produced uniformly short filaments, which led to improved magnetic properties, further underscoring the importance of precise control over filament length and morphology. The comparative studies between different protein scaffolds (γPFD and encapsulin) and their functionalized variants provided valuable insights into how protein architecture and functionalization affect the synthesis and properties of REE nanoparticles.

LIST OF SYMBOLS, ABBREVIATIONS, AND ACRONYMS

AFRL	Air Force Research Laboratory
M&P	Materials & Processing
RX	Materials & Manufacturing Directorate
RXE	Photonics, Electronics & Soft Materials Division
RXEB	Biomaterials Branch, Photonic, Electronic, and Soft Materials Division, Materials and Manufacturing Directorate
USAF	United States Air Force
WPAFB	Wright-Patterson Air Force Base